Multiscale Effects of Interfacial polymer Confinement in Silica Nanocomposites

H. Samet Varol [a*], M. Alejandra Sánchez [a], Hao Lu [a], Joe E. Baio [b], Christian Malm [a], Noemi Encinas [c], Marius R. B. Mermet–Guyennet [d], Nicolas Martzel [e], Daniel Bonn [d], Mischa Bonn [a], Tobias Weidner [a], Ellen H. G. Backus [a], Sapun H. Parekh [a*]

[a] Departments of Molecular Spectroscopy and [c] Physics at Interfaces, Max Planck Institute for Polymer Research, Ackermannweg 10, 55128 Mainz, Germany

[b] School of Chemical, Biological and Environmental Engineering, Oregon State University, Corvallis, Oregon 97333, United States

[d] Institute of Physics, University of Amsterdam, Science Park 904, 1098 XH Amsterdam, The Netherlands

[e] Manufacture française des pneumatiques MICHELIN, Site de Ladoux, 23 place Carmes Déchaux, 63040 Clermont Ferrand, France.

*E–mail varol@mpip–mainz.mpg.de (H.S.V)

*E–mail parekh@mpip–mainz.mpg.de (S.H.P)

Abstract: Dispersing hydrophilic nanofillers in highly hydrophobic polymer matrices is widely used to tune the mechanical properties of composite material systems. The ability to control the dispersion of fillers is closely related to the mechanical tunability of such composites. In this work, we investigate the physical – chemical underpinnings of how simple end –group modification to one end of a styrene – butadiene chain modifies the dispersion of silica fillers in a polymer matrix. Using surface–sensitive spectroscopies, we directly show that polymer molecular orientation at the silica surface is strongly constrained for silanol functionalized

polymers compared to nonfunctionalized polymers because of covalent interaction of silanol with silica. Silanol functionalization leads to reduced filler aggregation in composites. The results from this study demonstrate how minimal chemical modifications of polymer end groups are effective in modifying microstructural properties of composites by inducing molecular ordering of polymers at the surface of fillers.

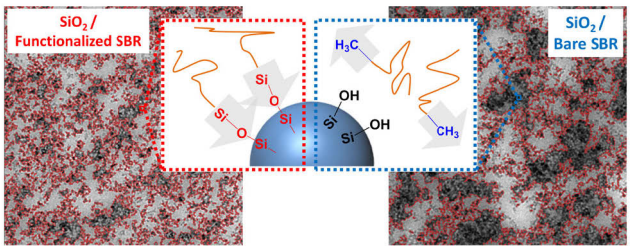

Introduction

For many natural and synthetic composite materials, enhancing or reinforcing the linear and nonlinear viscoelastic properties of polymer (elastomer) materials is accomplished by inclusion filler particles (e.g. carbon black, silica).[1–4] Mechanical properties of elastomer systems can be substantially increased, e.g., more than a 10–fold increase in shear modulus, by addition of fillers to the polymer matrix. Notably, this strengthening, or reinforcement, depends in a nontrivial manner on the distribution and size of fillers within the elastomer matrix.[5–7] Interfacial interactions between individual particles in aggregates, between the aggregates in agglomerates, and between particles and the polymer can modulate particle dispersion and influence the molecular motion of polymer chains in the material. Moreover, in nanocomposites containing nanoparticle fillers with large surface area, the particle dispersion is a critical element for tuning optical,[8,9] electrical[10–12], biological[13,14], and mechanical properties[15–19] of the materials. Unfortunately, controlling the filler distribution in many popular nanocomposite formulations, such as SiO_2–particle reinforced rubber, is challenging because the typically highly hydrophilic fillers tend to aggregate in the hydrophobic host polymer melt. Previous approaches to overcome the hydrophobicity difference between the matrix and fillers include: (1) covalent coupling of the fillers to the polymer matrix using multifunctional molecules, for instance bis[3–(triethoxysilyl)propyl] tetrasulfide (TESPT)[20–26] or (2) lowering the surface polarity of the hydrophilic fillers by surface modification with silanes,[27–29] short hydrocarbons[30,31], or polymer layers grafted on the filler surface.[32] A recently highlighted strategy for improving the dispersion of SiO_2 particles in styrene–butadiene rubber (SBR) is modifying the host SBR chains themselves with a single silanol functional group (Si–OH) at the end of the chain.[33–35] The appealing part of this concept is that the aggregate size (R_{agg}) of SiO_2 fillers can be varied in styrene–butadiene rubber (SBR) by simply changing the concentration of functionalized SBR (F–SBR) chains in the

total SBR matrix. However, the impact of polymer functionality on polymer–filler interaction – if any – is still unclear because of the complexity in previously studied systems and inability to investigate the polymer–substrate physicochemical properties.[34]

In this work, we investigate the influence of a single Si–OH end functional group on 50% of total SBR chain ends on polymer–silica interaction at the molecular level by studying well–defined systems with a combination of microscopy and surface–sensitive spectroscopy. We evaluate the adhesion and molecular ordering of both F-SBR and nonfunctionalized or bare SBR (B-SBR) polymers to SiO_2 surfaces. Our spectroscopic results demonstrate preferential adhesion of F-SBR chains to SiO_2 surfaces and directly show enhanced ordering of polymer chains in F–SBR–SiO_2 films compared with B–SBR–SiO_2 from surface specific sum frequency generation and near edge X–ray absorption fine structure spectroscopy. Finally, depth–resolved X–ray photoelectron spectroscopy was used to show that the Si–OH group formed a covalent bond with OH–terminated silicon surfaces. The multiscale effect of using the Si–OH functionalized SBR starts with covalent interaction between F-SBR and SiO_2 fillers that leads to increased polymer ordering and ultimately manifests as improved filler distribution and reduced aggregation at the microscopic level compared to B–SBR–SiO_2 composites.

Materials and Methods

Materials. For all composites fabricated in this study, we used nonvulcanized/non–crosslinked styrene butadiene rubber (SBR) polymers. Two types of SBR polymers were employed: 1) silanol end–functionalized SBR (F–SBR) and 2) bare SBR (B–SBR) polymers. Both polymers were synthesized in Michelin laboratories.[34] Initiation of anionic polymerization of both random F-SBR and B-SBR copolymers are done by using *n*–BuLi in a methlycyclohexane. *N*–(1,3–dimethylbuthyl)–*N'*–phenyl–*p*–phenylenediamine and 4,4*'*–methylene–bis–2,6–*tert*–

77 buthylphenol were used as antioxidants during the polymerization of both copolymers. Protic
78 terminating agent was used to terminate the B-SBR polymerization. Termination of the F-SBR
79 polymerization was obtained by reaction with hexamethylcyclotrisiloxane in order to have silanol
80 end group at one end of each F-SBR chain. Functionalized end–group of F-SBRcan be
81 chemically written as SBR–$SiMe_2$–OH. Functional group fraction in one end of all F-SBR chains
82 was reported previously as greater than 98% according to the results from ^{1}H and ^{29}Si NMR.[34] In
83 the same previous paper, microstructures of both polymers are also shown similar to each other
84 due to their identical polymerization steps. Each chain of both copolymers statistically consists of
85 26 wt % of styrene and 74 wt % of butadiene units (41 wt % of 1,2–butadiene and 59 wt % of
86 1,4–butadiene units).[34] These subunits are indicated in every molecular structure shown in the
87 paper by using the letters m, n, k and p for styrene, 1,2–butadiene and 1,4–butadiene (k+p, for
88 trans and cis), respectively. However, the ratio of $[1,4]_{trans}$ to $[1.4]_{cis}$ or k:p ratio is not known,
89 and it is not crucial for the content of this paper as it is the same for B-SBR and F–SBR. Gel
90 permeation chromatography (GPC) of the polymer showed the M_n and polydispersity index (PDI)
91 of both stock polymer solutions in THF (M_n~150–160 kDa, PDI~1.08–1.11) to be very similar to
92 each other, and very close to values previously reported for identical SBR polymers.[34] The
93 polymer chain stock solutions (40 mg/mL THF) were prepared by dissolving bulk slabs of B-
94 SBR and F-SBR in THF for 4 days at 4°C. The 4–day incubation time was necessary to
95 completely solubilize the polymers in THF.
96 Fumed Silica nanofillers (Aerosil 200, Evonik, R_0=6 nm were used as received to prepare a
97 stock solution. Silica particles were prepared as a stock solution (15.2 mg/mL THF) by ultrasonic
98 dispersion of the nanoparticles with a probe–type sonicator (half inch probe diameter, 10 s, 60%
99 amplitude, inside of an ice–bath) at room temperature.

100 **Nanocomposite formulation.** Formulation details of the full nanocomposites can be found
101 elsewhere.[34] Simplified nanocomposites were prepared according to the following protocol.
102 Silica fillers at a concentration of 45 per hundred rubber (PHR) or 16 % volume fraction of
103 nanofillers were mixed with the polymer solution. 5.920 mL nanofiller stock solution was added
104 to 5 mL of polymer chain stock solution. The final mixture was mixed with an ultrasonic tip (half
105 inch probe diameter) for 10 s at 60% amplitude while sitting in an ice bath. After mixing, initial
106 THF removal was done by rotary evaporation under 20 mbar for 30 min (Rotavapor R–200,
107 Buechi, Essen). Complete THF removal was done by keeping the samples in a vacuum oven at
108 80 °C for 24 h. In order to prevent reaction between end–functional Si–OH of F-SBR and the
109 surface of any glassware, we used only plastic ware for all the simplified nanocomposite sample
110 preparations.

111 **Transmission electron microscopy imaging and image processing.** All nanocomposite
112 samples were sectioned to a thickness of 50 nm by ultracryotome (LEICA EM UC6, Wetzlar) at
113 –60°C using a diamond knife (Cryotome ultra 35°, Hatfield, USA) for the transmission electron
114 microscopy (TEM) imaging. TEM micrographs were taken by operating a JEOL electron
115 microscope (JEOL JEM 1400, Eching) with an accelerating voltage of 120kV with constant
116 electron beam intensity and at a magnification of 5000X. We imaged a total 4000
117 aggregates/sample from different locations within each section to compute the average aggregate
118 size of the nanofillers (R_{agg}). The aggregates were determined by applying a thresholding routine
119 to highlight silica aggregates against the rubber background in each TEM image using ImageJ.
120 The following steps were followed: 1) OK Brightness and Contrast, 2) unsharp mask (radius was
121 set to 45 and mask weight was used as 0.6), 3) threshold with a value of the difference value
122 between mean and stdDev of each image, which can be found in histogram after the step 2, and

4) counting (from one primary filler to infinite size). This procedure was kept constant for all samples measured.

The output from the image analysis was: aggregate projected area (A), perimeter, and centroid location. We assume a circular shape with the measured projected area (A) for each aggregate from which we calculated the aggregate radius (R_{agg}).

Statistical analysis of image data. Statistical analyses from image processing were done with OriginPro using the ANOVA package. Aggregates from different fields–of–view for the same material (section) were grouped together, and the ANOVA procedure allows us to compare the variance in aggregate size for each sample to test if the mean value is statistically different from the other samples. The comparison test performed was Tukey, and significant differences between two samples are shown by a black asterisk, indicating a P value < 0.05.

Contact angle measurements. Teflon and silica window substrates were first cleaned by immersing in piranha solution (3:1 (v/v) H_2SO_4: H_2O_2) for 10 min then rinsed with milli Q water and absolute ethanol. The substrates were then left in a desiccator for 24 h for complete drying. Spin coating of the B-SBR and F-SBR films on Teflon and silica window surfaces were done by using a spin coating device Model WS–400–6NPP/LITE (Laurel Technologies Corp., North Wales, USA). 100 µL from each 40 mg/mL stock solutions of F-SBR and B-SBR were deposited on the substrates during 1 min at 3000 rpm. After the spin coating, the substrates with polymer films on the top were left in desiccator for 24 h.

For understanding a possible polarity difference between the B-SBR and F-SBR due to polymer functionality, we measured the contact angle of water as probe liquid on aforementioned spin coated polymer films on the top of Teflon or silica windows. The contact angle experiments were performed with an OCA35 goniometer (DataPhysics, Germany). The advancing contact angle of the spun coated rubber films was evaluated by placing an initial sessile droplet of milli Q water of

147 5 μL on the surfaces. The volume of the deposited droplet was increased up to 25 μL at a rate of
148 0.5 μL/s while keeping the needle in the drop. At the plateau regions of the contact angle (CA) in
149 increasing volume the advancing CA for water of the polymer films is obtained. Advancing CA
150 presented in Figure S7 are reported after averaging the mean values from at least two different
151 spot per spin coated film and three different plateaus (cycles) per each of these spots.

152 **Drop cast polymer film preparation and characterization.** Drop cast films of pure F-SBR or
153 B-SBR were prepared for various spectroscopy measurements in this study, and the following
154 method was used, 1500μL from each 40 mg/mL of polymer stock solutions were drop cast on
155 cleaned IR–transparent silica windows (Infrasil, International Crystal Laboraties, Garfield).
156 Windows were cleaned by following the previously mentioned piranha cleaning protocol of the
157 substrates for before the spin coating.

158 Teflon rings were used as molds for film casting. The drop cast polymer films were kept inside a
159 fume hood for 1 h before being transferred to a vacuum desiccator for 24 h in order to obtain
160 THF–free polymer films. After complete removal of the THF from the polymer, the residual dry
161 film thickness was found to be 150 μm – 180 μm by measurement with a microscope (IX81,
162 Olympus, Tokyo) using a 40X, NA 0.75 objective lens (Olympus, Tokyo).

163 **Infrared spectroscopy.** Fourier transform infrared spectroscopy (FTIR) was used to measure
164 characteristic peaks of the residual polymer films adhered to a piranha–cleaned silicon wafers and
165 absorption of IR light by polymer films on silica windows. Samples were measured with a
166 Nicolet 730 FTIR spectrometer. All FTIR spectra shown were averaged over three different
167 regions of the drop cast film. The integration time for the IR measurements was 800 s. Average
168 IR intensity values between the frequencies of 2120 cm^{-1} and 2140 cm^{-1} of each averaged FTIR
169 spectra were used for the background subtraction.

170 **Sum–frequency generation spectroscopy.** Sum frequency generation (SFG) experiments were
171 performed on the silica–polymer interface of drop–cast polymer films with broadband SFG
172 system in the following way. 1.7 mJ of energy from a Ti:sapphire regenerative amplifier (Spitfire
173 Ace, Spectra–Physics; 800 nm, 5 mJ, 1 kHz, ~40 fs) was used to pump a commercial optical
174 parametric amplifier (Topas–C, Spectra–Physics). This resulted in 4 μJ infrared (IR) pulses
175 centered at 3000 cm–1 with a full width at half maximum (FWHM) of ~400 cm–1. Visible
176 narrow band pulses with a center wavelength of 800 nm and FWHM of ∼15 cm–1 were obtained
177 by passing part of the 800 nm laser output through an etalon (SLS Optics Ltd). The IR and visible
178 beams were spatially and temporally overlapped on a film sample with incident angles of ~30°
179 (visible) and ~40° (IR) with respect to the surface normal. The energy of the visible and IR pulses
180 at the sample were 5 μJ and 3 μJ, respectively, to avoid sample damage. The reflected SFG signal
181 was directed to a spectrograph (Acton Instruments) and detected with an electron–multiplied
182 charge–coupled device (EMCCD) camera (Newton; Andor Technologies). Spectra were recorded
183 using Andor Solis software with an integration time of 10 min. All spectra where collected under
184 SSP polarization (s–polarized SFG, s–polarized visible, p–polarized infrared).
185 **SFG data analysis.** The SFG signal results from a second–order nonlinear interaction, which is
186 only non–zero in non–centrosymmetric media. This makes SFG especially useful to probe
187 interfacial phenomena where the interface between two media clearly breaks the symmetry, and a
188 finite SFG signal is generated that reflects the molecular composition and structure of the
189 interface. The SFG intensity is proportional to the square of the second order nonlinear
190 susceptibility $\chi^{(2)}$ of the sample and the visible and infrared electric fields

191 $$I_{SFG} = \left|E_{SFG}\right|^2 \propto \left|\chi^{(2)} E_{VIS} E_{IR}\right|^2 \qquad (1)$$

192 The SFG is enhanced when the frequency of the incident infrared field is resonant with a
193 vibrational mode present at the interface. The susceptibility $\chi^{(2)}$ consists of a resonant (RES) and
194 nonresonant (NR) term.

195 $$\chi^{(2)} = \chi^{(2)}_{NR} + \chi^{(2)}_{RES} = A_{NR} e^{i\varphi_{NR}} + \sum_n \frac{A_n}{\omega_{IR} - \omega_n + i\Gamma_n} \qquad (2)$$

196 where A_{NR} is the amplitude of the nonresonant susceptibility, φ_{NR} the phase, A_N the amplitude
197 of the nth resonance with frequency ω_n, and Γ_n the line width of the vibrational transition. To
198 correct for the spectral shape of the IR pulse, data were normalized to a reference spectrum from
199 a 100–nm evaporated gold layer on IR–transparent silica. Equation 3 was then used to fit the
200 normalized SFG spectra and extract the peak amplitudes and positions for the different
201 resonances. The Maximum Entropy Method for phase retrieval was used to verify the phase of
202 the peaks and the non–resonant signal[36]. All SFG spectra shown in this work are an average of 12
203 spectra (four spots on two independent samples).

204 **Near–edge X–ray absorption fine structure (NEXAFS) microscopy.** Near–edge X–ray
205 absorption fine structure (NEXAFS) microscopy was performed on the silica–polymer interface
206 of drop–cast polymer films; however, before placing the drop cast polymer films in the NEXAFS
207 analysis chamber, the bulk polymer layer was peeled off the silica window by using a fine
208 tweezer. This was done in order to analyze the thin polymer film in close proximity to the silica
209 surface.

210 NEXAFS images were collected at the U7 beamline at the National Synchrotron Light Source
211 (NSLS – Brookhaven National Laboratory). An X–ray beam, with energy scanned around the
212 carbon K–edge was raster scanned across an 18 × 13 mm^2 area on the sample. The spatially
213 resolved partial electron yield (PEY) was measured using a rapid imaging analytical tool

214 (LARIAT, Synchrotron Research Inc.). The step size for the scans was 0.1 eV (2 s dwell time).
215 The emitted photoelectrons were guided to an electron yield detector by a full field imaging
216 parallel magnetic field. This produced a series of NEXAFS images with a 50 μm spatial
217 resolution, which was used for the small spot analysis of different areas of the films. The spectra
218 shown are representative of four spots analysed on the sample surface. To eliminate the effect of
219 incident beam intensity fluctuations and absorption features in the beamline optics, the PEY was
220 normalized by the drain current signal of a clean gold mesh located upstream of the analysis
221 chamber along the path of the incident X–ray beam. All the images and spectra from NEXAFS
222 analysis in this paper have been pre– and post–edge normalized using the Athena software
223 package.

224 **Ultrathin spun coat polymer film preparation and X–ray photoelectron spectroscopy.** For
225 the XPS measurements, 20 μL drops from each 10 mg/mL F–SBR/THF and B–SBR/THF
226 solutions were deposited onto piranha cleaned Si wafers. These Si wafers with polymer solution
227 drops on the top were then spin coated for 60 s at 3000 rpm . After the spin coating, the samples
228 were kept under vacuum and then they placed inside of the XPS ultra high vacuum chamber. The
229 approximate thickness of the spin coat polymer films was determined using a KLA Tencar P–16
230 stylus profiler (KLA Tencar, Milpitas, California). XPS was conducted using a Kratos Axis Ultra
231 spectrometer (Kratos, Manchester, England) using an Al K*a* excitation source with a photon
232 energy of 1487 eV. An argon gas cluster ion source (GCIS) was used for depth profiling the
233 atomic composition of the polymer films (Figure S5). The sputter source was set to a raster size
234 of 1.5 mm × 1.5 mm, and ~200 etching steps were required to fully remove the 60 nm polymer
235 film.

236

237 The data was acquired in small spot mode (0.1 mm spot diameter) using a 0° take–off angle,
238 defined as the angle between the surface normal and the axis of the analyzer lens. The analyzer
239 pass energy was set to 80 eV for composition analysis. The molecular environment of the
240 samples was probed by high–resolution spectra (analyzer pass energy = 20 eV) from the C1s and
241 O1s regions. The charge neutralizer was always used during spectra collection (filament current
242 1.8 Å, charge balance 2 V, and filament bias 1.3 V). The binding energy scales were calibrated to
243 the main bulk Si 2p emission at 99.3 eV, and a linear background was subtracted for all peak
244 quantifications. The peak areas were normalized by the manufacturer supplied sensitivity factors
245 and surface concentrations were calculated using the Kratos Vision software.

246 1. Results and Discussion

247 1.1 Silanol Functional End Groups on Polymer Chains Modify SiO_2 Filler 248 Aggregation

249 The molecular structures of the two styrene – butadiene (SBR) polymers used in this work are
250 shown in Figure 1c (inset). The synthesis of the two polymers has been described previously, and
251 the basic protocol is summarized in the Methods.[34] The only difference between the two
252 polymers is a single silanol (Si–OH) end group on "functionalized" SBR (F–SBR), corresponding
253 to 1 Si–OH at the end of an ~ 150 g mol^{-1} SBR chain. The other polymer, with terminal methyl
254 groups, will further be referred to as "bare" SBR (B–SBR). In complex, industrial silica–filled
255 composites, F-SBR chains have been shown to substantially affect silica nanofiller aggregation
256 and distribution.[33,34] This difference is purported to occur via interaction of the Si–OH on the
257 polymer to the silica surface, which creates a brush around fillers to reduce the filler–filler
258 aggregation. This hypothesis is in line with previous studies that have shown that grafting of
259 polymer chains on silica surfaces reduces filler aggregation in hydrophobic environments.[24]

However, explaining the origin of changing nanofiller dispersions in SBR as a result of polymer functionality alone is not obvious in complex industrial formulations. They include many additional ingredients e.g. TESPT, octyltriethoxysilane (OCTEO), additional (proprietary) oils, and antioxidants, all of which can influence particle dispersion.[33,34]

To isolate the effect of silanol end–functional groups on filler aggregation in silica loaded SBR composites, we begin by analyzing the size distribution of silica aggregates (R_{agg}) in simplified nanocomposite systems. These composites contain only the polymer (F-SBR or B–SBR) and silica nanofillers (see Methods). Transmission electron microscopy (TEM) images of ultrathin sections (~ 50 nm) of simplified nanocomposite systems were acquired and processed to identify aggregates (dark contrast regions, see Methods for details) dispersed in the polymeric matrix (Figure. 1a). For comparison purposes, full nanocomposites were also imaged and processed to identify aggregates (Figure. 1b). We quantified the effective aggregate radius R_{agg} of each different composite by averaging the area of 4000 aggregates from each composite and assuming a circular shape, similar to what is done in small angle X–ray scattering. Figure 1c shows that in both full and simplified nanocomposites, samples containing F-SBR(red bars) have smaller aggregates than those with B-SBR(blue bars). We note that while TEM is certainly not the optimal choice for analysis of nanoscale aggregates in polymer matrices, we have compared our results with those from small angle X–ray scattering (SAXS) for full nanocomposite systems and find reasonable agreement at 16 % volume fraction with more dispersity at 24 % volume fraction (Figure S1). The thresholding step in our image analysis is subject to the image contrast between polymer and fillers (see Methods), and because the distance between aggregates decreases at higher filler volume fraction, this makes absolute aggregate size quantification less accurate at higher volume fraction. Furthermore, interpretation of aggregate sizes as a function of volume

fraction is difficult as competing effects (e.g. particle shearing and energetically–driven aggregation) can oppositely affect the aggregate size and disentangling these effects is challenging.[34,37,38] Nevertheless, the consistent reduction of aggregate size seen in F-SBR composites compared to B-SBR composites from both TEM image analysis and SAXS for 16% and 24% volume fraction filler demonstrates that our quantitative aggregate analysis is robust for comparing aggregate sizes at the same volume fraction with different polymer matrices (Figure. S1). Thus, our results show that, both in full and simplified composites, a single Si–OH end–functional group on an SBR polymer chain is able to modify the aggregation behavior of silica nanofillers in composite systems.

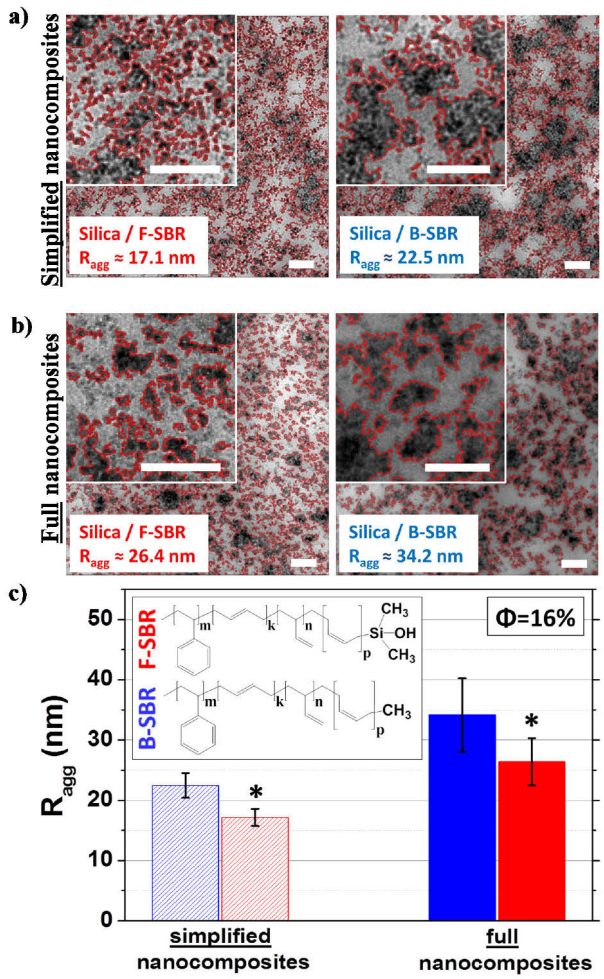

Figure 1. TEM images of (a) simplified nanocomposites, which consist of only nanoparticles inside polymer matrices and (b) the full nanocomposites (see ref [35] for detailed ingredients in addition to polymer chains and silica nanoparticles). Red outlines demarcate the borders of each aggregate after image analysis. All samples contain 16 vol. % of silica fillers in B-SBR or F–SBR. Scale bars are 200 nm. (c) Average aggregate sizes (R_{agg}) of simplified and full nanocomposites.

Red and blue bars represent R_{agg} of samples with F-SBR and B-SBR polymeric matrices, respectively. The inset shows the molecular structures of the two polymers. Letters, m, k, n and p represent the amounts of statistically ordered polymer units of both random copolymers (see Methods for the details). Histograms of the aggregate sizes of all the composites are presented as supplementary (Figure S2). Asterisks denote statistically significant differences ($p < 0.05$) of R_{agg} between B–SBR–silica and F–SBR–silica samples (1–way ANOVA with Tukey's). Error bars are standard error of mean.

1.2. Silanol Functional End Group Enhances Polymer Chain Attachment on SiO_2 Surfaces

To better understand the origin of the aggregate size decrease in silica/F-SBR samples, we compared the adhesion of B-SBR and F-SBR polymers with planar SiO_2 surfaces. Polymers were drop cast onto piranha–cleaned silicon wafers from a stock solution of polymer in THF (see Methods). Cleaned silicon wafers typically have a thin (SiO_2) oxide layer after piranha cleaning.[39–41] We tested if Si–OH groups on the F-SBR polymer increased attachment to the wafers by rinsing the polymer–coated wafers in a THF bath for 80 s. Since the polymers were initially dissolved in a THF solution, rinsing with THF should solubilize weakly adhered polymer chains in both B-SBR and F-SBR films. After this procedure, a visible film was left on the wafer

304 coated with F–SBR, but no film was observed on the B-SBR coated wafer (Figure. 2a). We
305 subsequently used Fourier transform infrared spectroscopy (FTIR) to determine the chemical
306 composition of the residual film on the F-SBR coated silicon wafer. Representative spectra from
307 the THF–washed wafers are shown in Figure 2b. These spectra confirm the presence of SBR after
308 THF rinsing for the drop cast F-SBR film while no chemical moieties (beyond those of the Si
309 wafer) were apparent for the corresponding B-SBR sample. From these data, we conclude that
310 attachment of the F-SBR polymer to the piranha–cleaned silicon wafer is clearly enhanced by the
311 single Si–OH group on the chains.

312

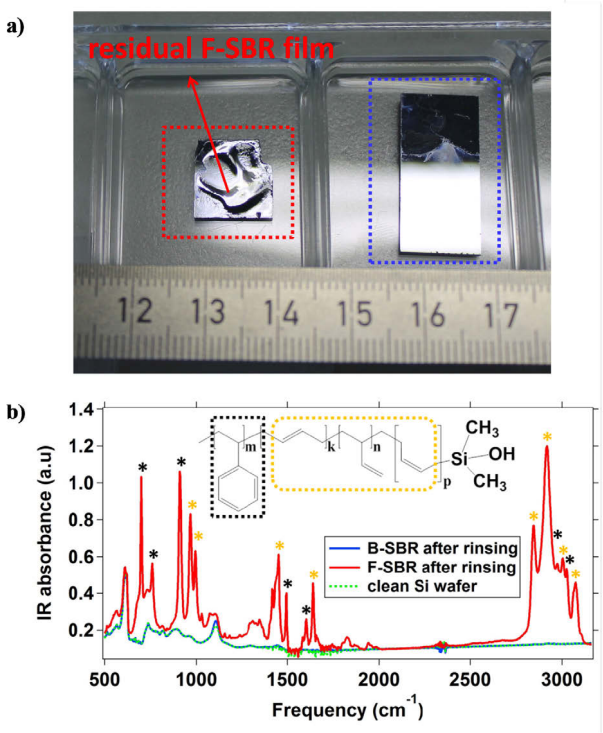

Figure 2. (a) Photographic images of F-SBR(left) and B-SBR(right) residue on silicon wafers after rinsing polymer films with THF. (b) FTIR spectra of residual films on Si wafer after rinsing in THF. Clear peaks from SBR are observed for the F-SBR polymer (red) while only Si wafer peaks (green–dashed) are seen after the B-SBR polymer (blue) has been rinsed. Characteristic groups of SBR are shown by outlines in yellow or black on the chemical structure. The same colours are used to identify particular vibrations (marked by asterisks) in the spectrum associated with each characteristic group.

314 ## 1.3. Molecular Ordering of Polymer Chains on SiO_2 from Silanol Functional End
315 Group Interaction with SiO_2 Surfaces

316 The enhanced attachment of F-SBR chains on silicon surfaces presumably originates from the Si–
317 OH group interacting with the SiO_2. We further explored the surface – polymer interaction to
318 determine if any differential molecular orientation was induced by Si–OH mediated attachment
319 of the F-SBR polymer to silica. Vibrational sum frequency generation (SFG) spectroscopy and
320 near edge X–ray absorption fine structure (NEXAFS) spectroscopy were used to measure
321 molecular order of the polymer at the silica surface.

322 SFG is a second order nonlinear vibrational spectroscopy that relies on frequency – mixing of an
323 infrared with a visible laser pulse to generate light with the sum frequency. The SFG intensity is
324 strongly enhanced when the infrared laser wavelength is resonant with molecular moieties (e.g.,
325 CH_2, C=C, or Si–CH_3 groups) that are present and noncentrosymmetrically oriented at an
326 interface. SFG has a typical probing depth of ~2–3 molecular layers[42] and has been used
327 extensively to characterize polymer films on various interfaces[43–48], making this technique well–
328 suited for our system. For SFG (and NEXAFS) experiments, we used drop cast films of B-SBR
329 and F-SBR on cleaned, infrared–grade silica windows – without THF washing. Silica windows
330 were used instead of wafers because visible light transparency is required for SFG experiments.

331 SFG spectra were collected from the silica window surface – polymer interface by passing the
332 laser beams through the silica to the silica–polymer interface as shown in Figure 3a. In principle,
333 polymer SFG signals should come from both the polymer–silica and polymer–air interfaces.
334 However, in these samples the polymer–air SFG signal is negligible because the infrared light in
335 the CH–region is strongly absorbed by the drop cast polymer layer (see Figure S3), so SFG is

336 only detected from the polymer–silica interface. SFG spectra were recorded under SSP

337 polarization conditions (s–polarized SFG, s–polarized visible and p–polarized IR).

338

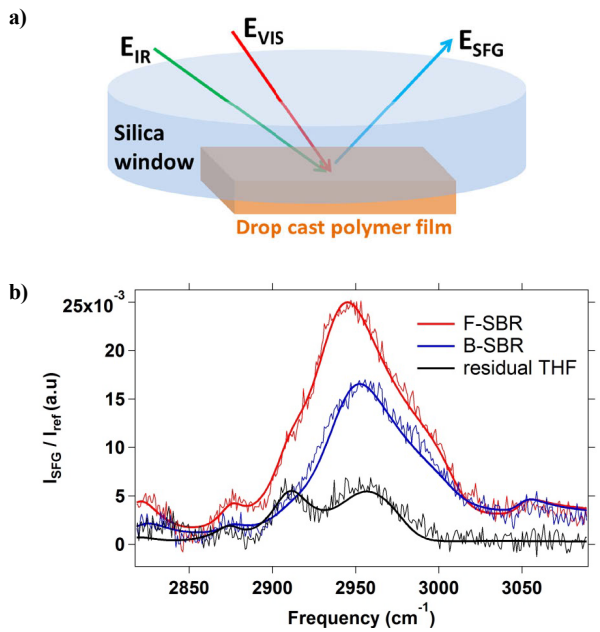

Figure 3. (a) Schematic illustration of the SFG measurements of drop cast polymer films on IR–transparent silica. Two incoming photons (infrared and visible shown by green and red arrows, respectively) are spatially and temporally overlapped at the window–polymer interface and generate a photon (E_{SFG}, shown by the blue arrow) with the sum of these frequencies. (b) Normalized (by a reference spectrum from a gold coated window) SFG spectra measured from F-SBR(red) and B-SBR(blue) and residual THF without polymer (black). Thick lines are fits to the spectra

based on a standard model (see Methods).

339

340 Figure 3b shows the SFG spectra from the F–SBR−silica interface in red and the B–SBR−silica
341 interface in blue. Spectra from both polymers indicate some degree of molecular order at the
342 silica interface as evidenced by the peaks in the spectra. Control spectra from a THF solution
343 dried on the silica window (without any polymer) showed a 300% and 500% decrease in intensity
344 at ~ 2950 cm^{-1} compared to B-SBR and F–SBR, respectively (Figure. 3b, black).

345 The spectra from the F–SBR–silica interface shows clear deviation from the B–SBR–silica
346 interface at ~ 2915 and 2950 cm^{-1}, in addition to a larger overall amplitude. In order to assign
347 peak frequencies and identify the specific moieties contributing to the spectra, we fit the SFG
348 data with a standard model explained in the Methods (using parameters that can be found in
349 Table S1). The fitting results are also depicted in Figure 3b (thick lines) and show good
350 agreement with the acquired data. The robustness of the fit was further demonstrated by
351 comparing the reconstructed resonant spectra from the fits with the extracted resonant spectra via
352 the commonly used maximum entropy method (MEM) analysis (Fig. S4).[36] These two
353 independent analyses show similar spectra, underscoring the accuracy of the fits to allow reliable
354 peak assignment.

355 From the fitting results and previous work on polymer– interfaces for polydimethylsiloxane
356 (PDMS) in contact with silica, we can identify likely resonances in the SFG spectra. The PDMS–
357 silica interface shows symmetric and asymmetric Si–CH_3 vibrations at roughly 2915 cm^{-1} and
358 2960 cm^{-1}.[49] Similarly, we assign the 2910 cm^{-1} shoulder and 2940 cm^{-1} peak in the F-SBR
359 spectrum to these two Si–CH_3 vibrations (Fig. 3b, red). In the B–SBR–silica sample, the broad

signal at 2945 cm^{-1} possibly originates from the CH_3 end group; however, a definitive assignment is not possible. Nevertheless, the identity of the peaks ($Si–CH_3$) in the F–SBR–silica system and the overall larger intensity (compared to B–SBR) show that the Si–OH group in F-SBR is in close proximity to the silica and stabilizes a conformation of the polymer in which the neighboring $Si–CH_3$ groups exhibit a noncentrosymmetric organization.

As a complementary technique to SFG, NEXAFS spectroscopy allows one to determine the spatial orientation of chemical structures based on absorption of a polarized X–ray beam by the sample.[50,51] NEXAFS spectra were measured on the same type of drop cast films as used for SFG measurements. Prior to introducing the samples into the NEXAFS analysis chamber, the bulk drop–cast polymer layers were physically ripped from the silica window, leaving behind a residual polymer film on the SiO_2 surface (Figure. 4a).

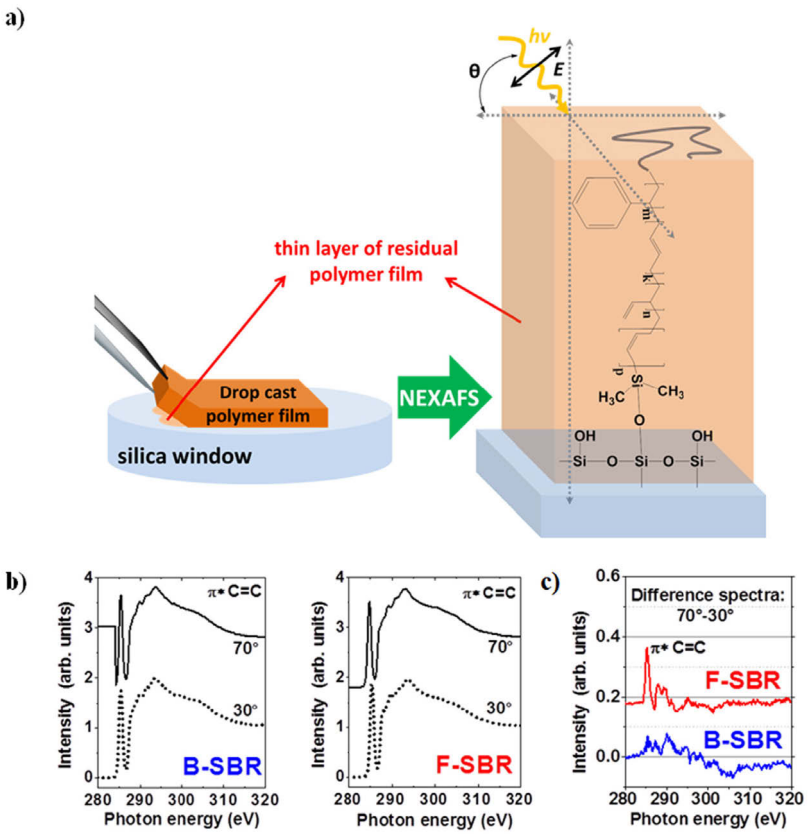

Figure 4. (a) Illustration showing removal of drop cast polymer films using tweezers before the NEXAFS measurements. Silica windows with the residual polymer film were introduced into the NEXAFS analysis chamber. Preferential orientation of molecules (e.g., π* C=C orbitals within SBR chain) to the silica surface can be determined from changes in X–ray absorption at different sample rotation (θ) relative to the incident X–rays. (b) Carbon K–edge spectra extracted from random regions of B-SBR(left) and F-SBR(right) residual films on silica acquired at 70° (straight lines) and 30° (dotted lines). (c) The difference spectra (70° – 30°) are shown in red and blue for F-SBR and B–SBR, respectively. Spectra in (b) and (c) were vertically offset for clarity.

NEXAFS spectroscopy probes the molecular structure of surface adsorbed species by measuring characteristic absorption resonances corresponding to electronic transitions from atomic core levels to unoccupied molecular orbitals.[51] Carbon K–edge spectra from randomly chosen regions

of interest of B-SBR and F-SBR residues on silica windows, acquired at 70° and 30° relative to the incident X–ray beam, are presented in Figure 4b. The absorption at 285.4 eV, from π* C=C orbitals, is present in all spectra taken from both types of polymers.[52,53] Moving to higher X–ray energies, we observe a shoulder at 288 eV and a broad resonance at 293 eV related to R*/C–H σ * and C−C σ * molecular orbitals, respectively.[53–56]

Preferential orientation of molecular bonds was investigated by subtracting spectra from 70° and 30° tilt angles. Difference spectra (70°–30°), from B-SBR and F-SBR residual films are shown in Figure 4c. A comparison of the two difference spectra (Fig. 4c) shows a substantially higher degree of order (positive dichroism) for the π* C=C feature for the F-SBR polymer residue interfaced with silica with a peak height of 0.2 at 285.2 eV. No significant dichroism was observed for the B-SBR residue–SiO_2 interface, especially in the π* C=C region of the difference spectrum (5–fold lower than for F–SBR). This shows that the functionalization of the SBR polymer with a single Si–OH induces a specific orientation of C=C double bonds, such that the C=C bonds are somewhat upright relative to the substrate.

1.4 Covalent Nature of the Interfacial Interaction Between Silanol Functional End Groups and Silica

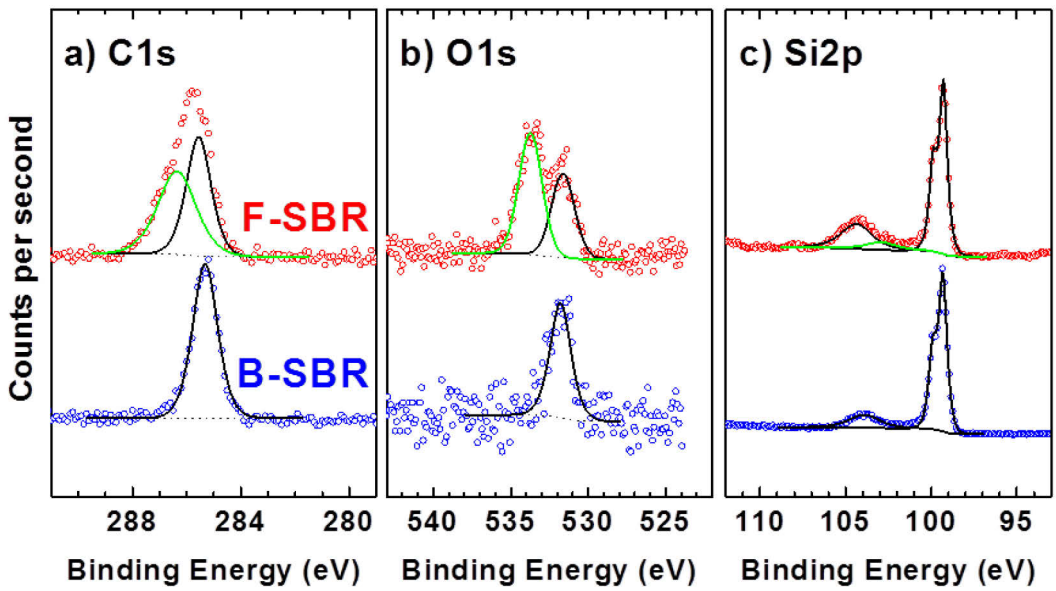

Figure 5. XPS spectra of the (a) C 1s, (b) O 1s and (c) Si 2p from the polymer–wafer interface along with fit results (see Methods for details) collected from the F-SBR(red) and B-SBR(blue) films. Argon cluster etching time for the B–SBR–Si wafer interface is between 180 – 360 s. The F–SBR–Si wafer interface XPS results were extracted from etching times between 210 – 390 s. Figure S5 shows atomic % for C 1s, O 1s, and Si 2p during the entire argon etching times for both polymer samples. In all the XPS spectral fits, green and black lines are additional and common peaks, respectively, for both polymers.

Our results show decreased silica aggregation, enhanced adhesion, and enhanced molecular ordering of F-SBR polymers at silica interfaces, relative to B-SBR polymers, as a result of the presence of the Si–OH end functional group on the F-SBR polymer. However, none of the above measurements have addressed the question how the Si–OH group interacts with silica:

398 chemisorption or physisorption. In order to address this question, we studied the elemental
399 composition and chemical state of the B-SBR and F-SBR polymer films spun cast onto piranha–
400 cleaned Si wafers using depth–resolved X–ray photoelectron spectroscopy (XPS). Spin–coated
401 polymer films (thickness ~ 60 nm) were depth profiled by repeated sputtering using an argon
402 cluster source and XPS analysis of the exposed surface (see Methods and Figure S5). This
403 process provides a snapshot of atomic concentrations (%) at different depths in the polymer film
404 as it is etched toward the substrate. By plotting the atomic concentration of Si and C versus etch
405 time, we can define a particular etching period that best reflects the polymer–substrate interface
406 (Figure S5).

407 The C 1s spectra of both F-SBR and B-SBR at the SiO_2 layer (which is present after piranha
408 etching silicon) show a main emission near 285.3 eV assigned to aliphatic and aromatic CC
409 bonds (Figure. 5a). [57–59] Spectral fitting reveals that the spectra for the F-SBR– SiO_2 interface
410 contain a second peak near 286.4 eV, which can be assigned to C–Si–O or Si–C bonds coming
411 from the Si–OH end functional groups at the end of F-SBRchains.[60–63] This additional peak
412 supports the conclusion from SFG that the Si–OH end functional groups are condensed at
413 polymer–Si wafer interface and not in the bulk film (Figure. S6a). Looking next at the
414 corresponding O 1s spectra of both polymers at SiO_2 layer, we observe a common peak at 531.8
415 eV originating from Si–O bonds at the Si wafer surface.[64,65] Similar to the C 1s spectra, we
416 identified an additional peak after fitting the O 1s spectrum for F-SBR(Fig. 5b). The second peak
417 near 533.7 eV can be assigned to Si–O–R and Si–O–Si bonds,[61,64,66] and appears only at the F–
418 SBR–silica interface – not in the bulk film (Fig. S6b).

419 This observation is corroborated by the Si 2p spectra shown in Figure 5c. The main spectral
420 features near 104.4 and 99.3 eV in both spectra related to Si–O–Si species within the thin oxide

421 layer[66–69] are accompanied by a peak near 102.7 eV – only in the F-SBR spectra. The latter peak
422 can be assigned to C–Si–O–Si.[60,64,68,70] Together, the additional peaks from C 1s (286.4 eV), O 1s
423 (533.7 eV) and Si 2p (102.7 eV) spectra at the polymer–substrate interface led us to the following
424 conclusions: (i) the $(CH_3)_2$–Si–OH end functional groups of F-SBR chains are enriched at the
425 surface of the Si wafer and not detectable in the bulk film and (ii) the formation of chemical
426 bonds between the Si–OH group and the silicon substrate, which leads to the formation of
427 $(CH_3)_2$–Si–O–Si moieties at the interface as the result of a condensation reaction.

428 ## Conclusion

429 In this work, we demonstrate that single Si–OH end groups on SBR chains are sufficient to
430 enhance the interaction of SBR chains with silicon and SiO_2. The increased interaction manifests
431 as stronger adhesion of the F-SBR chains to silicon surfaces as compared to B-SBR chains.
432 Together with increased adhesion, the additional interaction of the Si–OH functionalized polymer
433 with SiO_2 fillers ultimately led to reduced aggregation of the silica nanofillers within the SBR
434 matrix. The fact that the simplified and full composites showed similar reduced aggregation in F-
435 SBR compared to B-SBR polymers suggests polymer–filler interactions also contribute to
436 improving the dispersion of fillers in the more complex melt formulations as well. The idea of
437 grafting polymer chains to silica particle surfaces with end group modifications has been
438 previously demonstrated, though in the context of hydrophilic polymers, to study polymer
439 segmental motion at silica interfaces.[71–73] This is quite different from the current study in which a
440 hydrophobic rubber – SBR – was attached to silica using a terminal silanol group, which allows
441 identification of functional (aggregation) and physical chemical (molecular ordering) differences
442 when compared to methyl–terminated SBR.

443 To further explore the molecular origin of the improved adhesion of F-SBR chains to glass
444 surfaces, we employed multiple surface–specific spectroscopies. From these measurements, we
445 observed strong dichroism in carbon K–edge spectra from NEXAFS showing ordering of C=C
446 bonds in the F–SBR/silica system. Further experiments with SFG showed that the F–SBR–silica
447 interfaces exhibited Si–CH_3 signals that were larger than in B-SBR films. Finally, XPS spectra
448 showed covalent bonding of Si–OH groups with silicon substrates in F-SBR films. These
449 findings, along with the polymers having identical hydrophobicity (Figure. S7), show that
450 interaction of a single Si–OH group from the F-SBR polymer with the SiO_2 filler surface results

in polymer ordering at the silica surface, which thereby decreases filler aggregation in the nanocomposites. While it is possible that specific, covalent attachment of polymers to an interface can cause disorder in the case of multivalent attachment, the combined results from SFG and NEXAFS surface spectroscopies for F-SBR films demonstrate that covalently attached polymers are more ordered at the silica interface.[74,75] The results from this study provide a mechanistic basis for future attempts to directly graft hydrophobic host polymer matrices to hydrophilic fillers with aim of improving filler dispersion and mechanical properties of composite materials.

Author Information

Corresponding authors

varol@mpip–mainz.mpg.de

parekh@mpip–mainz.mpg.de

Acknowledgements

We acknowledge I. Lieberwirth, G. Glaser, and K. Kirchoff for assistance with TEM imaging and ultracryotome sample preparation. M.A.S thanks the Max Planck Graduate Center for funding. This work is part of the research programme 'Understanding the viscoelasticity of elastomer based nanocomposites' (11VEC01) of the' Stichting voor Fundamenteel Onderzoek der Materie (FOM)', which is financially supported by the' Nederlandse Organisatie voor Wetenschappelijk Onderzoek (NWO).

References

(1) Azouz, K. Ben; Ramires, E. C.; Van Den Fonteyne, W.; El Kissi, N.; Dufresne, A. *ACS Macro Lett.* **2012**, *1*, 236–240.

(2) McNally, T.; Pötschke, P.; Halley, P.; Murphy, M.; Martin, D.; Bell, S. E. J.; Brennan, G. P.; Bein, D.; Lemoine, P.; Quinn, J. P. *Polymer (Guildf).* **2005**, *46*, 8222–8232.

(3) Sapkota, J.; Jorfi, M.; Weder, C.; Foster, E. J. *Macromol. Rapid Commun.* **2014**, *35*, 1747–1753.

(4) Sternstein, S. S.; Zhu, A. J. *Macromolecules* **2002**, *35*, 7262–7273.

(5) Jancar, J.; Douglas, J.; Starr, F. *Polymer (Guildf).* **2010**, *51*, 3321–3343.

(6) Kalfus, J.; Jancar, J. *Polymer (Guildf).* **2007**, *48*, 3935–3937.

(7) Mermet–Guyennet, M. R. B.; Gianfelice de Castro, J.; Varol, H. S.; Habibi, M.; Hosseinkhani, B.; Martzel, N.; Sprik, R.; Denn, M. M.; Zaccone, A.; Parekh, S. H.; Bonn, D. *Polymer (Guildf).* **2015**, *73*, 170–173.

(8) Oberdisse, J. *Soft Matter* **2006**, *2*, 29.

(9) Jones, B. A.; Facchetti, A.; Marks, T. J.; Wasielewski, M. R. *Chem. Mater.* **2007**, *19*, 733–735.

(10) Winey, K. I.; Vaia, R. A. *MRS Bull.* **2007**, *32*, 314–319.

(11) Schadler, L. S.; Kumar, S. K.; Benicewicz, B. C.; Lewis, S. L.; Harton, S. E. *MRS Bull.* **2007**, *32*, 335–340.

(12) Moniruzzaman, M.; Winey, K. I. *Macromolecules* **2006**, *39*, 5194–5205.

(13) Rooney, M. M.; Farrell, D. H.; van Hemel, B. M.; de Groot, P. G.; Lord, S. T. *Blood* **1998**, *92*, 2374–2381.

(14) Lam, W. A.; Chaudhuri, O.; Crow, A.; Webster, K. D.; Li, T.–D.; Kita, A.; Huang, J.; Fletcher, D. A. *Nat. Mater.* **2011**, *10*, 61–66.

(15) Heinrich, G.; Klüppel, M.; Vilgis, T. A. *Curr. Opin. Solid State Mater. Sci.* **2002**, *6*, 195–203.

(16) Guth, E. *J. Appl. Phys.* **1945**, *16*, 20.

(17) McCarthy, D. W.; Mark, J. E.; Clarson, S. J.; Schaefer, D. W. *J. Polym. Sci. Part B Polym. Phys.* **1998**, *36*, 1191–1200.

(18) Dewimille, L.; Bresson, B.; Bokobza, L. *Polymer (Guildf).* **2005**, *46*, 4135–4143.

(19) Payne, A. R. *J. Appl. Polym. Sci.* **1965**, *9*, 2273–2284.

(20) Akcora, P.; Kumar, S. K.; Moll, J.; Lewis, S.; Schadler, L. S.; Li, Y.; Benicewicz, B. C.; Sandy, A.; Narayanan, S.; Ilavsky, J.; Thiyagarajan, P.; Colby, R. H.; Douglas, J. F. *Macromolecules* **2010**, *43*, 1003–1010.

(21) Chevigny, C.; Dalmas, F.; Di Cola, E.; Gigmes, D.; Bertin, D.; Boué, F.; Jestin, J. *Macromolecules* **2011**, *44*, 122–133.

(22) Chevigny, C.; Jouault, N.; Dalmas, F.; Boué, F.; Jestin, J. *J. Polym. Sci. Part B Polym. Phys.* **2011**, *49*, 781–791.

(23) Akcora, P.; Liu, H.; Kumar, S. K.; Moll, J.; Li, Y.; Benicewicz, B. C.; Schadler, L. S.; Acehan, D.; Panagiotopoulos, A. Z.; Pryamitsyn, V.; Ganesan, V.; Ilavsky, J.; Thiyagarajan, P.; Colby, R. H.; Douglas, J. F. *Nat. Mater.* **2009**, *8*, 354–359.

(24) Kumar, S. K.; Jouault, N.; Benicewicz, B.; Neely, T. *Macromolecules* **2013**, *46*, 3199–3214.

(25) Castellano, M.; Conzatti, L.; Costa, G.; Falqui, L.; Turturro, A.; Valenti, B.; Negroni, F. *Polymer (Guildf).* **2005**, *46*, 695–703.

(26) Hasegawa, R.; Aoki, Y.; Doi, M. *Macromolecules* **1996**, *29*, 6656–6662.

(27) Meth, J. S.; Zane, S. G.; Chi, C.; Londono, J. D.; Wood, B. A.; Cotts, P.; Keating, M.; Guise, W.; Weigand, S. *Macromolecules* **2011**, *44*, 8301–8313.

(28) Zhang, Q.; Archer, L. A. *Langmuir* **2002**, *18*, 10435–10442.

(29) Aranguren, M. I.; Mora, E.; Macosko, C. W. *J. Colloid Interface Sci.* **1997**, *195*, 329–337.

(30) Harms, S.; Rätzke, K.; Faupel, F.; Schneider, G. J.; Willner, L.; Richter, D. *Macromolecules* **2010**, *43*, 10505–10511.

(31) Nusser, K.; Neueder, S.; Schneider, G. J.; Meyer, M.; Pyckhout–Hintzen, W.; Willner, L.; Radulescu, A.; Richter, D. *Macromolecules* **2010**, *43*, 9837–9847.

(32) Radhakrishnan, B.; Ranjan, R.; Brittain, W. J. *Soft Matter* **2006**, *2*, 386.

(33) Baeza, G. P.; Genix, A.–C.; Degrandcourt, C.; Gummel, J.; Couty, M.; Oberdisse, J. *Soft Matter* **2014**, *10*, 6686–6695.

(34) Baeza, G. P.; Genix, A.; Degrandcourt, C.; Petitjean, L.; Schweins, R.; Couty, M.; Oberdisse, J. *Macromolecules* **2013**, *46*, 6621–6633.

(35) Baeza, G. P.; Genix, A.; Degrandcourt, C.; Petitjean, L. *Macromolecules* **2013**, *46*, 317–329.

(36) Sovago, M.; Vartiainen, E.; Bonn, M. *J. Phys. Chem. C* **2009**, *113*, 6100–6106.

(37) Kotsilkova, R.; Fragiadakis, D.; Pissis, P. *J. Polym. Sci. Part B Polym. Phys.* **2005**, *43*, 522–533.

(38) Baeza, G. P.; Genix, A. C.; Degrandcourt, C.; Gummel, J.; Mujtaba, A.; Saalwächter, K.; Thurn–Albrecht, T.; Couty, M.; Oberdisse, J. *ACS Macro Lett.* **2014**, *3*, 448–452.

(39) In, I.; La, Y.; Park, S.; Nealey, P. F.; Gopalan, P. *Langmuir* **2006**, *22*, 7855–7860.

(40) Yam, C.; Xiao, Z.; Gu, J.; Boutet, S.; Cai, C. *J. Am. Chem. Soc.* **2003**, *125*, 7498–7499.

(41) Leontis, I.; Othonos, A.; Nassiopoulou, A. G. *Nanoscale Res. Lett.* **2013**, *8*, 1–7.

(42) Nagata, Y.; Mukamel, S. *J. Am. Chem. Soc.* **2010**, *132*, 6434–6442.

(43) Wang, J.; Even, M. A.; Chen, Z. *Macromolecules* **2002**, *35*, 8093–8097.

(44) Loch, C. L.; Wang, J.; Chen, Z. *J. Phys. Chem. B* **2003**, *107*, 10440–10445.

(45) Loch, C. L.; Ahn, D.; Chen, C.; Wang, J.; Chen, Z. *Langmuir* **2004**, 5467–5473.

(46) Wang, J.; Chen, C.; Buck, S. M.; Chen, Z. *J. Phys. Chem. B* **2001**, *105*, 12118–12125.

(47) Wang, J.; Paszti, Z.; Even, M. A.; Chen, Z. *J. Am. Chem. Soc.* **2002**, *124*, 7016–7023.

(48) Chen, Z.; Shen, Y. R.; Somorjai, G. a. *Annu. Rev. Phys. Chem.* **2002**, *53*, 437–465.

(49) Zhang, C.; Chen, Z. *J. Phys. Chem. C* **2013**, *117*, 3903–3914.

(50) Baio, J. E.; Jaye, C.; Fischer, D. A.; Weidner, T. *Anal. Chem.* **2013**, *85*, 4307–4310.

(51) Stöhr, J. *NEXAFS Spectroscopy*; Springer Science & Business Media, 1992.

(52) Himmel, H.–J.; Terfort, A.; Wöll, C. *J. Am. Chem. Soc.* **1998**, *120*, 12069–12074.

(53) Outka, D. A.; Stöhr, J.; Rabe, J. P.; Swalen, J. D. *J. Chem. Phys.* **1988**, *88*, 4076.

(54) Väterlein, P.; Fink, R.; Umbach, E.; Wurth, W. *J. Chem. Phys.* **1998**, *108*, 3313.

(55) Weiss, K.; Bagus, P. S.; Wöll, C. *J. Chem. Phys.* **1999**, *111*, 6834.

(56) Baio, J. E.; Weidner, T.; Brison, J.; Graham, D. J.; Gamble, L. J.; Castner, D. G. *J. Electron Spectros. Relat. Phenomena* **2009**, *172*, 2–8.

(57) Afzal, A.; Siddiqi, H. M.; Saeed, S.; Ahmad, Z. *RSC Adv.* **2013**, *3*, 3885.

(58) Gulino, A.; Lupo, F.; Fragalà, M. E.; Schiavo, S. L. *J. Phys. Chem. C* **2009**, *113*, 13558–13564.

(59) Puniredd, S. R.; Assad, O.; Haick, H. **2008**, 13727–13734.

(60) Liu, Z. C.; He, Q. G.; Xiao, P. F.; Liang, B.; Tan, J. X.; He, N. Y.; Lu, Z. H. *Mater. Chem. Phys.* **2003**, *82*, 301–305.

(61) Shao, Y. X.; Dong, D.; Cai, Y. H.; Wang, S.; Ang, S. G.; Xu, G. Q. *J. Phys. Chem. C* **2010**, *114*, 17159–17165.

(62) Roghani–Mamaqani, H.; Haddadi–Asl, V. *Polym. Int.* **2014**, *63*, 1912–1923.

(63) Sengupta, R.; Chakraborty, S.; Bandyopadhyay, S.; Dasgupta, S.; Mukhopadhyay, R.; Auddy, K.; Deuri, a S. *Polym. Eng. Sci.* **2007**, *47*, 21–25.

(64) Mani, G.; Johnson, D. M.; Marton, D.; Dougherty, V. L.; Feldman, M. D.; Patel, D.; Ayon, A. a.; Mauli Agrawal, C. *Langmuir* **2008**, *24*, 6774–6784.

(65) Armstrong, J. L. *J. Vac. Sci. Technol. A Vacuum, Surfaces, Film.* **1998**, *16*, 123.

(66) Li, S. H.; Zhu, X. F.; Zhao, Y. P. *J. Phys. Chem. B* **2004**, *108*, 17032–17041.

(67) Schildenberger, M.; Prins, R.; Bonetti, Y. C. *J. Phys. Chem. B* **2000**, *104*, 3250–3260.

(68) Azioune, A.; Carpi, N.; Fink, J.; Chehimi, M. M.; Cuvelier, D.; Piel, M. *Langmuir* **2011**, *27*, 7349–7352.

(69) Vanden Eynde, X.; Servais, J. P.; Lamberigts, M. *Surf. Interface Anal.* **2003**, *35*, 1004–1014.

(70) Kannan, A. G.; Choudhury, N. R.; Dutta, N. K. *Polymer (Guildf).* **2007**, *48*, 7078–7086.

(71) Glomann, T.; Schneider, G. J.; Allgaier, J.; Radulescu, a.; Lohstroh, W.; Farago, B.; Richter, D. *Phys. Rev. Lett.* **2013**, *110*, 1–5.

(72) Glomann, T.; Hamm, A.; Allgaier, J.; Hübner, E. G.; Radulescu, A.; Farago, B.; Schneider, G. J. *Soft Matter* **2013**, *9*, 10559.

(73) Kim, S. Y.; Meyer, H. W.; Saalwa, K.; Zukoski, C. F. *Macromolecules* **2012**, *45*, 4225–4237.

(74) Weidner, T.; Krämer, A.; Bruhn, C.; Zharnikov, M.; Shaporenko, A.; Siemeling, U.; Träger, F. *Dalton Trans.* **2006**, 2767–2777.

(75) Glebe, U.; Weidner, T.; Baio, J. E.; Schach, D.; Bruhn, C.; Buchholz, A.; Plass, W.; Walleck, S.; Glaser, T.; Siemeling, U. *Chempluschem* **2012**, *77*, 889–897.